Available online at www.sciencedirect.com

ScienceDirect

Journal of Magnesium and Alloys 7 (2019) 58–71

www.elsevier.com/locate/jma

Review

Kinetics in Mg-based hydrogen storage materials: Enhancement and mechanism

Qun Luo[a,1], Jianding Li[b,1], Bo Li[b], Bin Liu[a], Huaiyu Shao[b,*], Qian Li[a,*]

[a] *State Key Laboratory of Advanced Special Steel & School of Materials Science and Engineering & Materials Genome Institute & Shanghai Key Laboratory of Advanced Ferrometallurgy, Shanghai University, 99 Shangda Road, Shanghai 200444, China*

[b] *Joint Key Laboratory of the Ministry of Education, Institute of Applied Physics and Materials Engineering (IAPME), University of Macau, Macau SAR, China*

Received 14 October 2018; received in revised form 5 December 2018; accepted 10 December 2018
Available online 28 December 2018

Abstract

Mg-based materials have been intensively studied for hydrogen storage applications due to their high energy density up to 2600 Wh/kg or 3700 Wh/L. However, the Mg-based materials with poor kinetics and the necessity for a high temperature to achieve 0.1 MPa hydrogen equilibrium pressure limit the applications in the onboard storage in Fuel cell vehicles (FCVs). Over the past decades, many methods have been applied to improve the hydriding/dehydriding (H/D) kinetics of Mg/MgH_2 by forming amorphous or nanosized particles, adding catalysts and employing external energy field, etc. However, which method is more effective and the intrinsic mechanism they work are widely differing versions. The hydrogenation and dehydrogenation behaviors of Mg-based alloys analyzing by kinetic models is an efficient way to reveal the H/D kinetic mechanism. However, some recently proposed models with physical meaning and simple analysis method are not known intimately by researchers. Therefore, this review focuses on the enhancement method of kinetics in Mg-based hydrogen storage materials and introduces the new kinetic models.

Keywords: Magnesium alloys; Hydrogen storage materials; Hydriding/dehydriding reactions; Kinetics.

1. Introduction

The rapidly depletion of traditional fossil fuel and public-concerned environmental problems have led to the development of clean and sustainable energy. Hydrogen is thought to be a promising alternative energy media for replacing the long-term use of fossil fuel while with no emitting CO_2 emission, but just water. However, the technologies for high density and low cost storing hydrogen are still to be solved. It is reported that solid-state storage materials can store atomic hydrogen in metal-based compounds resulting in relatively higher energy density and greater safety when compared with that of compressed gas storage and low-temperature liquid storage both stored with molecular hydrogen. These solid-state storage materials consist of metal hydrides, some complex hydrides and chemical hydrides [1–9]. For hydrogen-energy process chain and hydrogen economics, the new method that one-step approach is recommended which towards hydrogen generation and storage in $NaBH_4$ using Mg/MgH_2 [10–12]. In addition, Mg-based materials have been intensively studied for hydrogen storage applications due to the outstanding merits, such as the high hydrogen storage capacity (7.6 wt.% for MgH_2), low cost (2–3 USD kg^{-1}) and abundant resources in the earth's crust and the sea [13–15]. Fig. 1a presents the energy density of MgH_2 comparing with other materials. The energy density of MgH_2 can reach up to 2600 Wh/kg or 3700 Wh/L (calculated from the lower heating value of hydrogen), which shows clear advantage in comparison with other materials. Unfortunately,

* Corresponding authors.
E-mail addresses: hshao@umac.mo (H. Shao), shuliqian@shu.edu.cn (Q. Li).
[1] Equally contributing first author.

https://doi.org/10.1016/j.jma.2018.12.001

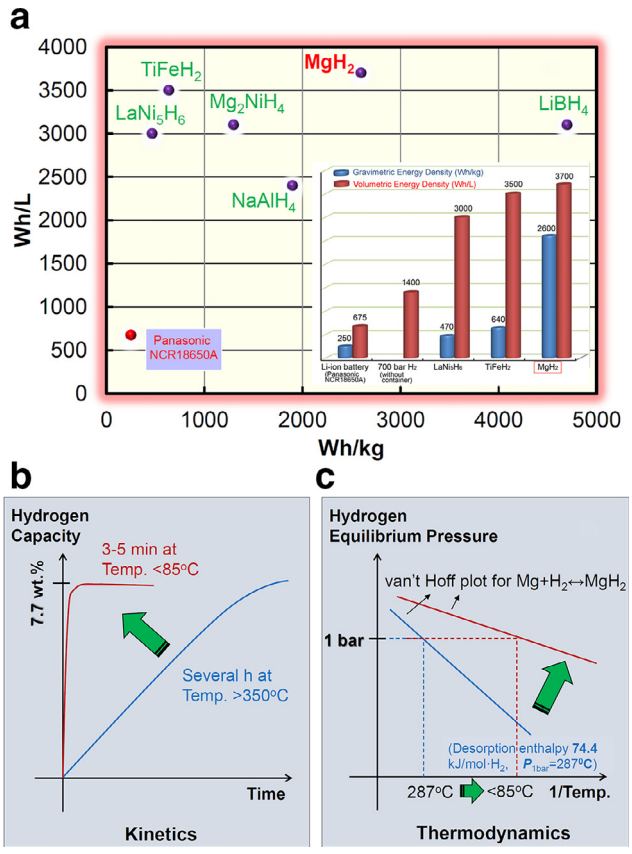

Fig. 1. (a) Energy densities of MgH_2 and their comparison with NCR 18650A lithium-ion battery, 70 MPa compressed hydrogen, and several other hydrogen storage materials, schematic illustration of the kinetic (b) and thermodynamic (c) requirements for onboard hydrogen storage and the current status in Mg–MgH_2 hydrogen-storage materials. Reprinted with permission [1].

the Mg-based materials with poor kinetics and the necessity for a high temperature to achieve 0.1 MPa hydrogen equilibrium pressure limit the applications in the onboard storage in FCVs [1].

2. Current situation of Mg-based materials for hydrogen storage development

As mentioned above, the challenges of the rigorous kinetics and the improper thermodynamics for Mg-based hydrogen storage materials hinder their possible onboard application, which needs high temperature and pressure to improve the properties [1,11,16-19]. Clearly, the current Mg-based hydrogen storage materials take hours to complete the hydrogen absorption reaction at a temperature of over 623 K under a hydrogen pressure over 3 MPa [20] (Fig. 1b). However, a refilling time of 3–5 min and max delivery temperature of 358 K are desired for on-board hydrogen storage in the hydrogenation process, which is a challenge for common Mg-based hydrogen storage materials. Concerning to the thermodynamics, the temperature for releasing 1 bar hydrogen is 560 K according to the desorption enthalpy (–74 $kJ \cdot mol^{-1}$ H_2) and entropy (–135 $J \cdot K^{-1} \cdot mol^{-1}$ H_2) in Mg-based materials (Fig. 1c). This

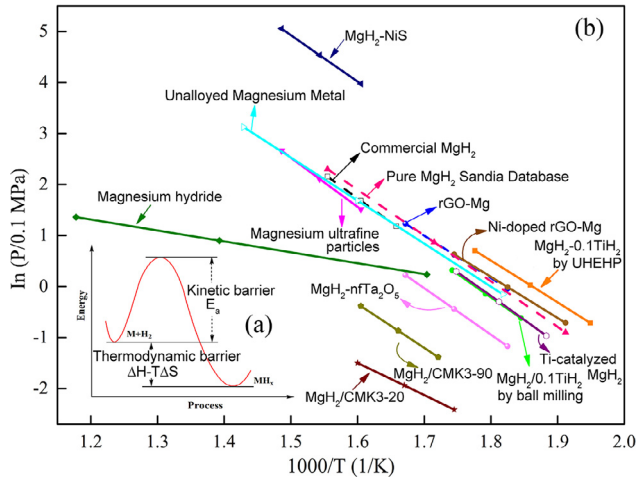

Fig. 2. (a) Schematic illustration of thermodynamic and kinetic barrier for de-/hydriding reactions of metal hydrides and (b) the van't Hoff plots of the desorption reaction for various Mg–MgH_2 systems. Reprinted with permission [16,22].

must be changed to release hydrogen at a temperature below 358 K [1].

It is known that the improper thermodynamics may be stemmed from the strong bonding of Mg–H for Mg-based hydrogen storage materials. The thermodynamics stability could be characterized by the formation enthalpy (ΔH) and entropy (ΔS) of metal hydride, while the kinetics barrier could be expressed by the activation energy of reaction (E_a). Moreover, the formation enthalpy and entropy also could be derived from the van't Hoff equation while the activation energy of reaction could be determined by Arrhenius or Kissinger's equation [21,22]. Herein, tailoring the thermodynamics and kinetics of hydrogenation/desorption reactions, as well as the van't Hoff plots of desorption reaction for various Mg–MgH_2 systems are showed in Fig. 2. It is concluded that the positive effect of downsizing and catalyst on the kinetics is widely accepted by the researchers, while for the downsizing effect on the thermodynamics of hydrogen absorption and desorption for Mg–MgH_2 system, different results are reported. In order to directly understand the relationship between the thermodynamics and the particle size, many van't Hoff equations for Mg–MgH_2 systems were presented. From Fig. 2b, we could see that there is no apparent change of thermodynamic properties in desorption reactions when downsizing the diameter from 5 to 300 nm. Shao et al. [16] focused on the effects of downsizing and the doping of additives (transition metals, metal oxides, halides, etc.) on the thermodynamics and kinetics of hydrogen desorption. It is found that there are no apparent changes of thermodynamic properties in desorption reaction with the catalyst and nanostructure on the scale down to 5 nm [23]. The ab-initio Hartree–Fock and density functional theory calculations suggest that both Mg and MgH_2 become less stable with decreasing cluster size, but MgH_2 is more destabilized than Mg upon decreasing the cluster size below 19 Mg atoms [24]. That is to say, a MgH_2 crystallite size of 0.9 nm would correspond to a desorption temperature of only 473 K.

Because the thermodynamic properties are hardly to be changed, many researchers focused on the improvement of hydrogenation and dehydrogenation kinetics. With regard to quantitatively evaluating the hydrogenation and dehydrogenation rate, the hottest topic focuses on the in-depth understanding of the H/D kinetic mechanism. The analysis of hydrogenation and dehydrogenation behavior by kinetic models is a significant and efficient way to reveal the kinetic mechanism. The evaluated kinetic triplet including the E_a, the pre-exponential factor (A) and kinetic model functions ($g(\alpha)$) quantificationally reflect the improvement effects. Up to now, a large number of kinetic models have been proposed [25–27],but only several classical models are frequently used, such as Jander model [28], Ginstling–Brounshtein function [29] and Johnson–Mehl–Avrami–Kolmogorov model [30–34]. The main problem concentrates on following aspects: (i) the kinetic function is too complicate to use, which only give the analytical solutions and cannot give the numerical solutions. (ii) The detailed assumptions and derivation steps are hardly found, which usually leads to misunderstanding of kinetic mechanism. (iii) It is difficult for the researchers to select the reasonable method among those numerous models to analyze their experimental data. In order to solve above problems, a series of formulae concerning the isothermal kinetics of gas-solid reaction based on a real physical picture are proposed in our previous work [35–39], which shows higher accuracy and provides more kinetic information. Therefore, the systematical summary of present kinetic model is provided to introduce the new analysis methods.

3. Enhancement of kinetics in Mg-based hydrogen storage materials

3.1. Nano and amorphous processing

Nano processing for the synthesis of nanosized Mg-based materials has gained more and more interest because of the need to increase the surface contact between Mg and hydrogen and to reduce the diffusion distance for hydrogen in particles and grains, which improves the hydrogen storage kinetics when the size is reduced to a few nanometers. Up to now, many methods are adopted to prepare the nanostructured Mg-based materials, including ball milling, thin film synthesis, catalyzed chemical solution synthesis, hydrogen plasma metal reaction, hydrogen combustion synthesis, nano-confinement, etc.

Ball milling is the most common technique to synthesize the hydrogen storage materials, which consists of mechanical grinding, mechanical alloying and reactive ball milling. The ball-milled materials with superior nano-size were formed when the strong force generated in the process of ball milling was applied to the composites inside. It is known that the method of ball milling has two advantages. One is that the time of ball milling is relatively shorter on account of usually reducing the particle size without atom rearrangement. The other is that it will introduce amounts of defects, dislocations and fresh surfaces of the samples, which will improve the chemical reactive activities in the gas phase, chemical solution or electrolyte. Moreover, the samples of micro-strain generated during the ball milling will decrease the effect of hysteresis in the cycling of absorption and desorption.

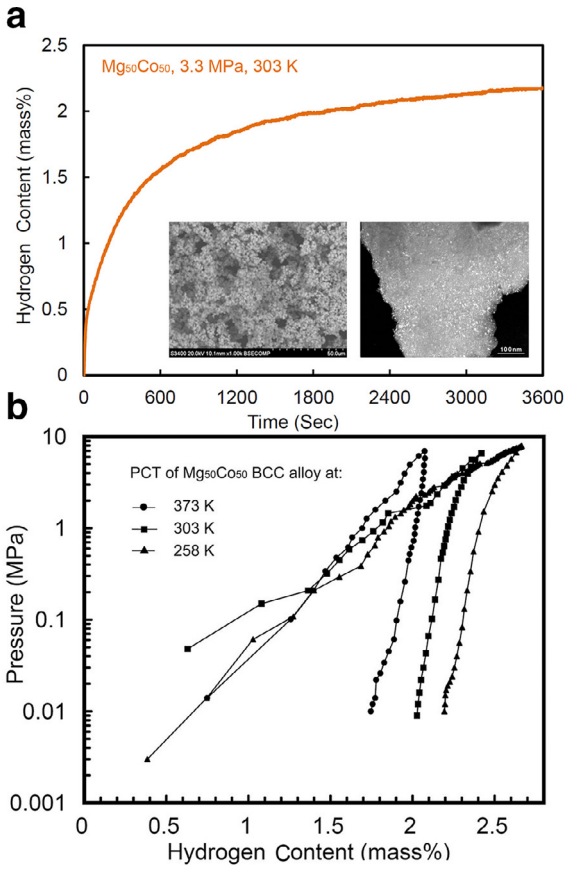

Fig. 3. (a) Hydrogen absorption curve of $Mg_{50}Co_{50}$ alloy at 303 K under an initial hydrogen pressure of 3.3 MPa (the insets are SEM image (left) and dark-field TEM image (right) of the alloy); (b) Pressure–composition isotherms of $Mg_{50}Co_{50}$ bcc alloy measured at different temperatures. Reprinted with permission [17,41].

Shao et al. [17,40,41] ball-milled the mixture of magnesium powder and cobalt powder at the rotation speed of 200 rpm for varying times from 0.5 to 400 h and then carefully investigated the phase, morphology, hydrogen storage properties and mechanism of nanostructured $Mg_{50}Co_{50}$ materials. The fabrication process of $Mg_{50}Co_{50}$ alloy is confirmed as $Mg + Co\text{-hcp} \rightarrow Mg_{nano} + Co_{nano}\text{-hcp} \rightarrow Mg_{nano} + Co_{nano} - hcp + Co_{nano}\text{-fcc} \rightarrow bcc + Co_{nano}\text{-fcc} \rightarrow bcc$. The as-obtained $Mg_{50}Co_{50}$ alloy is with 1–2 μm and the crystal size is about a few nanometers from the TEM image in Fig. 3a. It is interesting to mention that the $Mg_{50}Co_{50}$ alloy with bcc structure exhibited a higher hydrogen storage capacity at relatively lower temperature, which absorbs 2.67, 2.42 and 2.07 wt.% at 258, 303 and 373 K (Fig. 3b), respectively. The absorption temperature of 258 K is the lowest temperature reported for the Mg–Co composite. Two factors including the mechanical alloying and the bcc structure with proper lattice parameter are responsibility for the novel hydrogen storage performance.

The new developed ball-milling process assisted by dielectric-barrier discharge plasma for dual-tuning the thermodynamics and kinetics of Mg based hydrogen storage materials is deserved to mention [42–46]. This method solved the preparation problem of Mg(In) and Mg(In, Al) solid solution, moreover improved the preparation efficiency [42,43]. The dehydriding kinetics is modified via the catalyzing effect of in situ synthesized MgF_2. The dehydrogenation enthalpy change and activation energy of $Mg_{85}In_5Al_5Ti_5$ alloy were lowered to 65.2 kJ·mol^{-1} H_2 and 125.2 kJ·mol^{-1} [46], respectively. Ding et al. [47] reported a method for using hydrogen-induced Mg–Zr interfacial coupling to manipulate the migration of hydrogen atoms, thus significant enhanced the kinetics along with the thermodynamics of Mg–Zr–H MCs.

Beside the ball milling, the method of catalyzed chemical solution synthesis is also adopted to synthesize the Mg-based hydrogen storage materials. Bogdanovic et al. [48] fabricated the homogeneously catalyzed hydrogenation of magnesium with the raw materials of magnesium powders, anthracene, tetrahydrofuran and $CrCl_3$ or $TiCl_4$ acted as catalyst by the method of catalyzed solution synthesis for the first time. After that, Shao et al. [49] synthesized the nanostructured Ti-catalyzed nanocrystalline magnesium hydride by adopting this technique and fully studied its hydrogen storage properties. The typical procedure to prepare the Ti-catalyzed nanocrystalline magnesium hydride is listed in equations of (1)–(3).

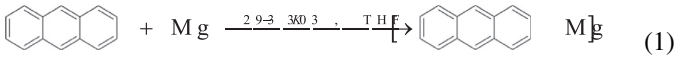

(1)

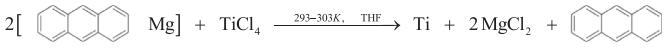

(2)

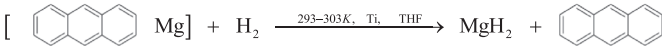

(3)

Rietveld analysis showed that the as-obtained sample made up of a tetrahedral β-MgH_2 phase with 89 wt.% and an orthorhombic high-pressure modification γ-MgH_2 with 11 wt.%. It is worth mentioning that it was the first time to observe the high-pressure modification γ-MgH_2 under such mild conditions. The re-hydrogenation of the two kinds of dehydrogenated MgH_2 was investigated, which was depicted in Fig. 4. Clearly, the Ti-catalyzed nano-Mg could absorb hydrogen at the temperature of 530, 545 and 573 K while the commercial Mg could absorb hydrogen at 573, 598 and 623 K under the same conditions. In addition, 6 wt% hydrogen could be absorbed in less than 1 h for the Ti-catalyzed nano-Mg, which is at least two times faster than that of the commercial Mg reaching the same capacity. The enthalpy and entropy values of hydrogen desorption for the nano-MgH_2 extracted from the equilibrium plateaus of the desorption measurements are 77.7 kJ·mol^{-1} H_2 and 138.3 J K^{-1}·mol^{-1} H_2, respectively, which means thermodynamic properties do not change with nanostructure and catalyst. The absorption

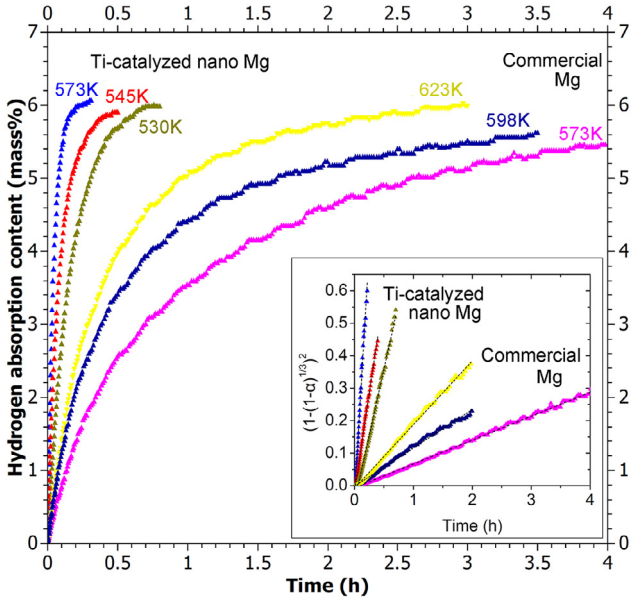

Fig. 4. Hydrogen re-absorption curves of Ti-catalyzed MgH_2 nanocrystalline sample and commercial MgH_2 sample (Alfa Aesar) at different temperatures in 1 MPa hydrogen after complete desorption (inset: absorption curves simulated by Jander diffusion equation). Reprinted with permission [17,49].

curves fitted by Jander diffusion equation were also shown in Fig. 4. The results indicated that the rate-limiting step was three-dimensional diffusion of hydrogen through the hydride. In addition, the absorption rate of Ti-catalyzed nano-Mg at 573 K was 3.06 s^{-1}, which was 40 times faster than that of commercial Mg (0.0736 s^{-1}).

Fig. 5 depicted the TEM images of the obtained metal and Mg-based alloys synthesized by hydrogen plasma metal reaction (HPMR) [17,50–53]. From the figures, it could see that the Ni, Cu, Co, Fe and Al particles had a granular structure and the particle size was with a mean size of 30–50 nm. While the Mg particles exhibited hexagonal structure and the average particle size was about 300 nm. When compared the size of Mg particles with other metals, it could clearly find that the Mg particles were much bigger than the other metal nanoparticles which was originated from the much faster vaporization rate and the higher generation rate of Mg than the ones of Ni, Co, Cu, Fe and Al metals [54]. Additionally, the Mg-based alloy were also obtained by HPMR. From the TEM micrographs, the obtained Mg_2Ni, Mg_2Co and Mg_2Cu were with an average size about 50–200 nm, which was smaller than that of original Mg particles. This indicated that the Mg–M mixture particles would crack into smaller ones during the hydrogenation and dehydrogenation process.

Fig. 6 presented the hydrogen absorption kinetics of Mg-based nanoparticles synthesized by HPMR methods. From Fig. 6a, it could see that the Mg nanoparticles could absorb hydrogen very quickly at 573 K after one absorption-desorption cycle under 4 MPa hydrogen pressure at 673 K. Moreover, the hydrogen absorption rate became faster as the temperature increasing. The hydrogen content increased greatly with the time and quickly reached a maximal value 7.54 wt.% in 30 min at 573 K. The nanostructured Mg_2Ni sam-

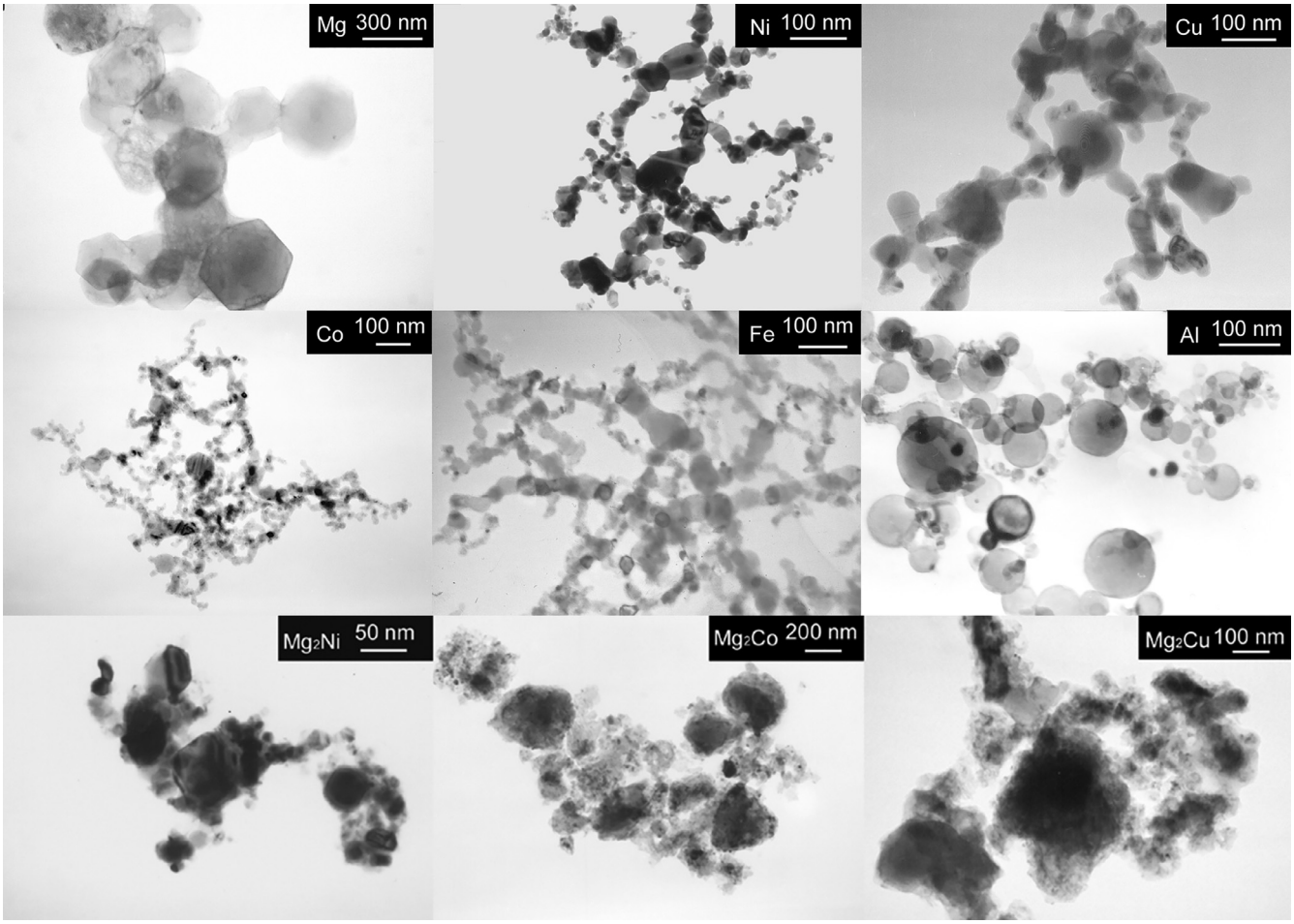

Fig. 5. TEM images of Mg, Ni, Cu, Co, Fe, Al metal nanoparticles and Mg_2Ni, Mg_2Co, Mg_2Cu alloys synthesized by hydrogen plasma metal reaction [17,50].

ple and $Mg_{85}Ni_{15}$ samples absorbed hydrogen with smaller hydrogen capacity but with a much faster speed than the Mg nanoparticle sample at the same temperature of 573 K. After 13 min absorption at 573 K under an initial hydrogen pressure of 3.5 MPa, the $Mg_{85}Ni_{15}$ nanocomposite sample showed a hydrogen capacity of 4.73 wt.%. With the existence of the nanostructured Mg_2Ni phase in the $Mg_{85}Ni_{15}$ sample, it could act as catalyst to the absorption reaction of Mg phase. The Mg_2Ni nanoparticle sample might even absorb hydrogen at room temperature (1.73 wt.% after 32 min absorption under 4 MPa H_2). Seen from Fig. 6b, there is no obvious delegation in the hydrogen absorption capacity and speed for the Mg_2Ni nanoparticle sample in 5 cycles at 623 K, which presented good cycle ability of the sample for hydrogen storage application. We knew normally Mg-based materials needed a strict activation process before they might absorb hydrogen with a fast rate and a reasonable hydrogen capacity at temperature above 523 K. These results demonstrated that superior hydrogen absorption kinetics and capacity of the Mg and Mg–M based nanoparticle samples.

Hydriding combustion synthesis (HCS) method is a common method that used to synthesize the nanosized hydrogen storage materials. Li et al. [55–63] prepared a series of Mg–RE–Ni nano-composites including $La_{1.5}Ni_{0.5}Mg_{17}$, $LaNiMg_{17}$, Mg-8 mol% $LaNi_{0.5}$, $Mg_{1.9}Al_{0.1}Ni$, Mg_2Ni, etc. using mechanically alloying and hydriding combustion synthesis method. These alloys showed much better hydrogenation and dehydrogenation kinetics than pure Mg. Yao et al. [64] coated $Mg_{95}Ni_5$ with polyvinylpyrrolidone (PVP) via HCS followed by wet mechanical milling with tetrahydrofuran. The $Mg_{95}Ni_5$–7 wt.% PVP nano-composites exhibited significant improved dehydriding kinetics, which was mainly due to the synergistic effect of PVP and THF. The addition of PVP and THF helps to alleviate the aggregation of Mg and MgH_2 particles during milling process. The dehydriding peak temperature of MgH_2 was reduced to 523 K and the dehydrogenation apparent activation energy was reduced to 66.94 $kJ{\cdot}mol^{-1}$ as well. The oxide-free $Al_{12}Mg_{17}$ on the surface of Mg particles was prepared by HCS and heating to 693 K [65]. The hydrogen firstly reacted with the newly generated $Al_{12}Mg_{17}$ and subsequently the hydrogen diffused into the inner part of the particles to further hydriding upon decreasing to 613 K and holding for 2 h under 1.5 MPa H_2 pressure. The promoted hydrogenation kinetics of Mg–10at.% Al composite was obtained by forming $Al_{12}Mg_{17}$ during HCS [65,66].

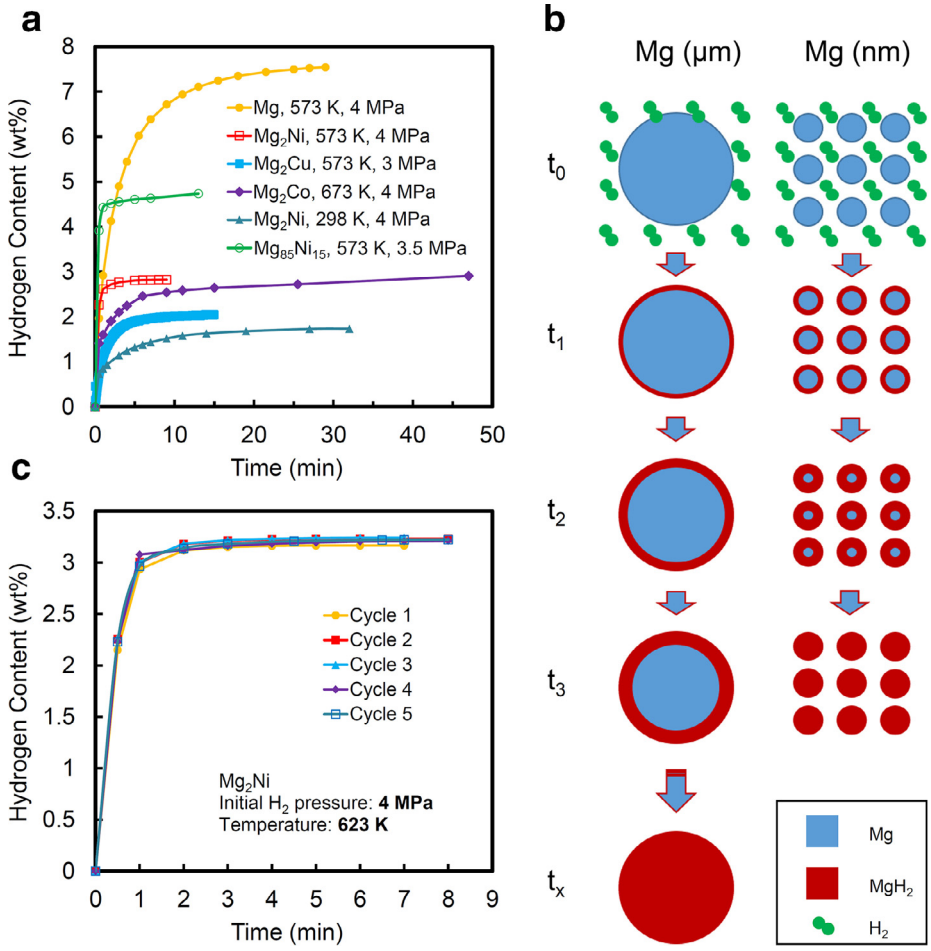

Fig. 6. (a) Hydrogen absorption curves of various Mg–M based nanoparticle samples (Mg, Mg_2Ni, Mg_2Cu, Mg_2Co and $Mg_{85}Ni_{15}$), (b) Absorption curves in five cycles of the Mg_2Ni nanoparticle sample, (c) A schematic showing effect of nanosizing on absorption kinetics in hydrogen storage materials. Reprinted with permission [17].

Nano-confinement is that utilization of nanoporous materials as scaffold for geometrically confining Mg-based hydrogen storage materials in nanoscale, which can inhibit the particle sintering or agglomeration during hydrogenation/dehydrogenation at elevated temperatures [67]. The onset dehydrogenation temperature of MgH_2–Ni@C composite is 460 K, which is 113 K lower than that of as-milled MgH_2 [68]. The $Mg@Ni_8Gn_2$ composite absorbs 6.28 wt.% of hydrogen in 100 s at 373 K and desorbs 5.73 wt.% of hydrogen in 1800 s at 523 K, suggesting that the composites have high hydrogen capacity and impressive fast kinetics in both hydrogenation and dehydrogenation [69]. Tan and co-workers introduced multi-walled carbon nanotubes supported titania (TiO_2/MWCNTs) into $Mg_{95}Ni_5$ [70], MWCNTs not only can act as lubricant during mechanical milling process, but also improve the dispersibility of TiO_2 nanoparticles and facilitate the diffusion of the H atom. The MWCNTs supported bimetal palladium and nickel co-catalyst showed hydrogen absorption capacity of 6.44 wt.% within 100 s at 373 K and hydrogen desorption capacity of 6.41 wt.% within 100 s at 523 K [71]. Chen et al. [72,73] prepared the Mg nanowires by vapor-transport approach. The results showed that thinner Mg/MgH_2 nanowires have a much lower desorption energy than that of thicker nanowires or bulk Mg/MgH_2, indicating the changes of kinetics and thermodynamics are expected when the diameters of nanowires are less than 30 nm. Zhang et al. [74] reported a novel strategy named microencapsulated nanoconfinement to realize local synthesis of nano-metal hydrides, which possesses ultrahigh structural stability and superior desorption kinetics. Monodispersed Mg_2NiH_4 single crystal nanoparticles were in situ encapsulated on the surface of graphene sheets via hydriding chemical vapor deposition. The MgO coating layer with a thickness of about 3 nm efficiently separated the nanoparticles from each other, preventing aggregation during hydrogen absorption/desorption cycles, leading to excellent thermal and mechanical stability. More interestingly, the MgO layer showed superior gas-selective permeability to prevent further oxidation of Mg_2NiH_4, meanwhile accessible for hydrogen absorption/desorption. As a result, an extremely low activation energy (31.2 $kJ \cdot mol^{-1}$) for the dehydrogenation reaction was achieved.

Amorphous processing is a novel method to prepare the Mg-based materials as a new hydrogen-storage pathway in comparison with that of crystalline ones, which was discovered in the 1960s [75]. Amorphous Mg-based alloys, such as Mg–RE–Ni, have attracted great interest because

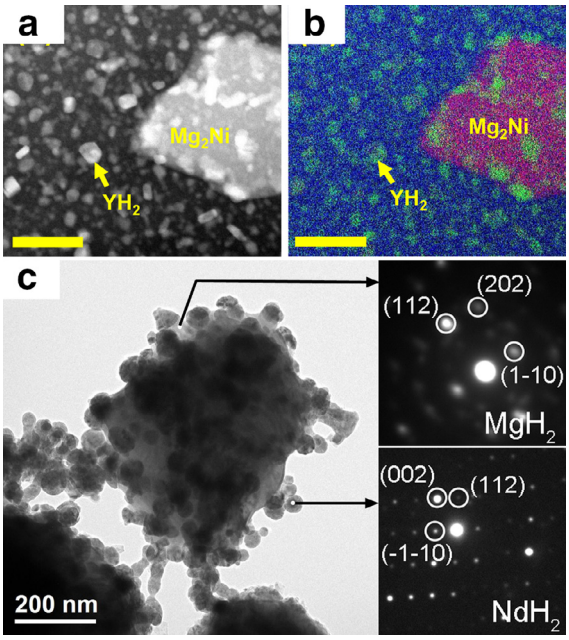

Fig. 7. (a) HAADF image of the $Mg_{12}NiY$ alloy after hydrogenation for 90 min, (b) EDS mapping of the area shown in (a), (c) the bright image of $Nd_4Mg_{80}Ni_8$ alloy and SAED pattern of NdH_2 and MgH_2. Reprinted with permission [83,85].

of the hydrogen storage capacity as high as in the case of MgH_2 (7.6 wt.%). Lin et al. [76] reported a hydrogen-induced glass-to-glass transition in amorphous $Mg_{80}Ce_{10}Ni_{10}$ alloys with a hydrogen storage capacity of about 5 wt.%. The enhancement of hydrogen storage capacity of this amorphous $Mg_{80}Ce_{10}Ni_{10}$ is attributed to the free volume and disordered atomic structure inside the material. Remarkably, the desorption temperature of the amorphous Mg–Ce–Ni can be efficiently tuned through the doping of 5at.% Cu with reduction from about 623 K to 423 K. It also indicated that the synthesis of nanoporous amorphous alloys could contribute to the hydrogen absorption properties [77].

Besides above-mentioned methods, recently, a new method of in-situ formation of REH_x–Mg–Mg_2Ni nanocomposites was developed through directly hydrogenation of the rare earth containing alloys. Zhu et al. [78-80] found that the composites of $CeH_{2.73}$−MgH_2–Ni and YH_2−Mg−$Mg_2NiH_{0.3}$ exhibited superior hydrogen storage kinetics. However, the as-melted $Mg_{80}Ce_{18}Ni_2$ alloy was a multiphase mixture which was composed of 57 wt.% $CeMg_3$, 29 wt.% Ce_2Mg_{17}, 7 wt.% CeMg and 5 wt.% $CeMgNi_4$ [78]. That is to say, the catalytic elements Ce and Ni did not distribute uniformly in the alloy, which would lead to the non-uniformity of in situ formed $CeH_{2.73}$−MgH_2–Ni composites. Therefore, Li et al. [81–83] proposed the method that direct hydrogenation of the single-phase Mg–RE alloy to form REH_x homogenously distributed Mg-based nanocomposites. The in situ formed YH_2 and NdH_2 grains with size less than 35 nm were interdispersed in the Mg and Mg_2Ni matrix (as shown in Fig. 7), which produced high density grain boundaries for the diffusion of H atoms. Although the enthalpy and entropy of hydrogenation/dehydrogenation of Mg were basically unchanged, the homogenous YH_2/NdH_2−Mg−Mg_2Ni nanocomposites showed excellent hydriding/dehydriding kinetics even after 620 [84] and 819 [85] cycles, respectively. Furthermore, the hydrogen storage capacity only decayed about 20% from the maximum value of 5.2 wt.%. The fast formation process of YH_2 in 18R-type LPSO phase is due to the high affinity between hydrogen atoms and the $L1_2$–Ni_6Y_8 clusters [83]. The in situ formed NdH_{3-x} nanograins could capture H atoms and transfer them from the 4b sites of NdH_{3-x} to the octahedral interstitial site of the NdH_{3-x}/α-Mg interface along the [1–100] direction [85].

To better understand the effect of downsizing on the kinetics, the mechanism for nanosizing on the hydrogen absorption kinetics in Mg-based materials is illustrated in Fig. 6c [86]. The hydrogenation was one of process of formation of hydrides in the Mg-based particles based on the reaction between Mg-based materials and hydrogen on the surface of the particles. The figure clearly shows that the nanostructured Mg can fully absorb hydrogen in a shortened time, which was faster than that of Mg with a size of micrometer. The nanostructured Mg with faster absorption kinetics may be attributed to larger surface area and smaller particle size [1,87,88], which means that Mg nanomaterials had a much greater contact area for hydrogen reaction, and a much shorter diffusion distance for hydrogen diffusion during the hydrogen absorption reaction [17,46,89,90]. Mg-based materials with the particles size in nanoscale could improve hydrogen storage kinetics even thermodynamics when the size was reduced to a few nanometers.

3.2. Additives with catalytic effects

Besides improving the kinetics with the reduction of particle size, catalytic additives were also combined with Mg-based materials to enhance the kinetics of absorption and desorption. Up to now, many publications related to the catalyzed Mg-based hydrogen storage materials have been reported, such as metal oxides [91–93], transition metals [40,52,53,94–98], rare earth elements [99,100], fluorides [101], halides [102–104], etc. Numerous efforts have been devoted to developing efficient catalyst for Mg-based hydrogen storage and some appear to be good.

Barkhordarian and collaborators [105] firstly reported the Nb_2O_5 catalysts doped MgH_2 by ball milling. The doped presented the fastest hydrogen sorption kinetics among these selected metal oxides. 6.9 wt.% of hydrogen could be absorbed within 60 s and the absorbed hydrogen could be fully desorbed in only 140 s. Clearly, the Nb_2O_5 dopant possessed the fastest desorption rate in comparison with that of other dopants, yielding a desorption rate of 0.011 wt.%/s. It is suggested that the metal with multiple valencies and catalytic effect of electronic exchange reacting with hydrogen molecular are attributed to the acceleration of the gas-solid reaction. In a word, the additive of Nb_2O_5 presented improved hydrogenation-dehydrogenation reaction for hydrogen storage. Mustafa et al. [106] reported the hydrogen storage properties of the ball-milled MgH_2 + 5 wt.% CeO_2 at the

speed of 400 rpm in an argon atmosphere. The results showed that the hydrogenation rate of CeO_2 doped MgH_2 composites was faster than of pristine magnesium hydride. The as-received MgH_2 at 593 K could absorb 3.46 wt% hydrogen after 5 min. In contrast, the hydrogen capacity of as-milled MgH_2 and MgH_2+5 wt% CeO_2 at 593 K could reach up to 3.72 wt.% and 3.95 wt.% after 5 min, respectively. In addition, about 3.6 wt.% hydrogen is released within 30 min for MgH_2+5 wt.% CeO_2 composites while less than 1.0 wt.% hydrogen for pure MgH_2. Moreover, the activation energies of the CeO_2 doped MgH_2 composite and pure MgH_2 are determined to be 133.62 and 108.65 $kJ{\cdot}mol^{-1}$, respectively, which indicated that the introduction of CeO_2 could lead to a great hydrogen desorption improvement. In a word, the enhanced performance of hydrogen storage is due to the formation of CeH_2 and CeO_2 species.

Extensive investigations have focused on the addition effect of transition metals (Ni [107,108], Nb [109], Ti [110], Fe [111]) and rare earth elements (RE = La [112], Ce [113], Pr [114], Nd [115], Sm [116]). The addition of Ti and Ni was found to play key role in improving the thermodynamic and kinetic properties of MgH_2 by decreasing the desorption temperature and the activation energy [117]. Mg–TM(Ti, Fe, Ni)–La ternary ultrafine particles produced by arc plasma method shows significantly improved hydrogen absorption kinetics and the hydrogen desorption temperature was reduced in the hydrogenated ternary Mg–TM–La composites when compared to those in the binary Mg–TM or Mg–RE composites [118]. The Mg–La–Fe–H nano-composites prepared through reactive ball milling can absorb 5.0 wt.% of hydrogen at room temperature and desorb hydrogen at 463 K [119]. NbH_x nanoparticles with disordered structure and small particle size (10–50 nm) were synthesized by ball milling $NbCl_5$ and LiH, and significantly enhanced the hydriding and dehydriding kinetics of MgH_2, which could desorb 7.0 wt.% H_2 within 9 min at 573 K and absorb ~4.0 wt.% H_2 at 373 K at a reasonable rate [120].

Due to the multiple alloy elements are introduced, seeking for the Mg-based multicomponent alloys with good hydrogen storage properties is time-consuming through traditional trial-and-error method. Therefore, the researchers take advantage of the phase diagram to design the novel hydrogen storage alloys [121–126]. Li et al. [81,127-129] assessed the phase equilibria of RE–Mg–Ni–H (RE = La, Ce, Y, Nd) systems at the Mg–Ni rich side. They used the phase diagram to discuss synthesized technological parameter of alloys and developed a series of Mg-based hydrogen storage alloys with good hydriding/dehydriding properties. A successful case of designing the Mg-based hydrogen storage alloy is the development of $Nd_4Mg_{80}Ni_8$ intermetallic compound by exploring the Nd–Mg–Ni–H phase diagram [81,82]. Based on the materials design idea that searching for the alloy with catalytic elements distribute uniformly in the whole sample, the attention was focused on Mg-based ternary intermetallic compound and the new phase $Nd_4Mg_{80}Ni_8$ was developed fulfilling the design requirement. The hydrogen-induced decomposition of $Nd_4Mg_{80}Ni_8$ led to in situ formation of $NdH_2-Mg-Mg_2Ni$ nanocomposites, which processed excellent hydrogenation and dehydrogenation kinetic properties and excellent cycling stability [85].

Since the property of fluorides is similar with chlorides and bromides, fluorides are also expected to be effective catalysts for the promotion of hydrolysis reaction. Doping MgH_2 with $NiCl_2$ and $CoCl_2$, both the dehydrogenation temperature and the absorption/desorption kinetics were improved, and a significant enhancement was obtained in $NiCl_2$ doped sample [130]. Mao et al. [101] produced a series core-shell structured Mg–MF_x (M = V, Ni, La, and Ce) nano-composites and tested the hydrolysis properties of corresponding hydrogenated powders. The results revealed that the addition of MF_x improves the hydrogen absorption kinetics and enhances its hydrolysis properties. Wei et al. [131] systematically investigated the catalytic actives of VF_4 on the hydriding cycling performance and dehydriding properties of $Mg_{99}Ni$. It demonstrated that the HCS+MM−$Mg_{99}Ni$+VF_4 could absorb 5.57 wt.% H_2 at 373 K in 50 s even after the 5th hydriding cycle and can release about 6.50 wt.% H_2 at 533 K within 1800 s and at 543 K within 1300 s, respectively. The formation of $VH_{0.91}$ phase during mechanical milling process played an important role on the improvement of dehydriding properties and hydriding cycling properties of the HCS + MM-$Mg_{99}Ni$.

Besides the simple substance, mixtures of complex hydrides were able to effectively modify MgH_2 system with high hydrogen capacity. MgH_2 doped with 2.5 wt.% $LiAlH_4$ and 2.5 wt.% $LiBH_4$ started to release H_2 at about 553 K and released a high hydrogen capacity of 7.62 wt.% with superior reaction kinetics, as well absorbed 7.7 wt.% H_2 within 15 min at 573 K. This synergistic effect of $LiBH_4$ and $LiAlH_4$ was ascribed to the in situ formation of Li_3Mg_7, $Mg_{17}Al_{12}$, and $MgAlB_4$, which acted as the "catalytic active sites" to facilitate the diffusion of hydrogen through the reaction barriers in the de/hydrogenation cycles of MgH_2 [132].

The catalytic effectiveness is not only determined by intrinsic activity but also the distribution state of the catalyst. The core-shell Mg-based nano-composites with shell-shaped catalysts are welcome in hydrogen storage materials. Zou et al. [133] produced a Mg-based Mg–La–O nano-composite with an arc plasma method followed by passivation in air. TEM analysis showed that such Mg ultrafine particles were covered by MgO and La_2O_3 nano particles, forming a core-shell structured metal-oxide composite. Then, they synthesized Mg–RE composite metal-oxides, such as Mg–Nd, Mg–Gd, and Mg–Er [134]. It shows that these RM-oxides can act as channels for hydrogen sorption, leading to a significant improvement of hydrogen sorption kinetics of Mg ultrafine particles. Lu et al. [135] produced a core-shell structured Mg@TM (TM = Co, V) composites via an approach combing arc plasma method and electroless plating. The measured hydrogenation enthalpy (− 70.02 $kJ{\cdot}mol^{-1}$ H_2) and activation energy (67.66 $kJ{\cdot}mol^{-1}$ H_2) of the ternary Mg@Co@V composite were lower than those of binary composites and the pure Mg powder. These improvements can be attributed to (i) the core-shell structure which may providing more nucleation sites for hydrogen sorption, and (ii) the co-effect of

Mg–Co hydrides. Binary Mg@Fe [136], Mg@Ti [137] and ternary Mg@Ti@Ni [137] have been synthesized in the same way. Mg_2FeH_6@MgH_2 core–shell hydrides comprised of the Mg_2FeH_6-core with a particle size of 40–60 nm and the MgH_2-shell with a thickness of 5 nm were synthesized, which released 5.1 wt.% H_2 within 10 min at 573 K, and 5.0 wt % H_2 within 50 min at 553 K. These low hydrogen desorption temperature and improved desorption kinetics were ascribed to the special core–shell nanostructure, leading to the dehydrogenation of the MgH_2-shell followed by the decomposition of the Mg_2FeH_6-core into Mg and Fe. The recovered core–shell nanostructure after rehydrogenation further contributed to the excellent cycling hydrogen desorption properties [138].

Carbon-wrapped transition metal (Co/C, Ni/C) nanoparticles (8–16 nm) were found a better catalytic efficiency when doped in the MgH_2 system. MgH_2-6% Co/C could release about 6.1 wt.% H_2 at 523 K and uptake 5.0 wt.% H_2 at 373 K within 20 s [139]. Mechanistic research revealed that the catalytic mechanism lied in the in situ formed Mg_2Ni and Mg_2NiH_4 nanoparticles acting as advanced catalytically active species and carbon attached around the surface of transition metal nanoparticles inhibiting the aggregation of the catalysts. Furthermore, $Na_2Ti_3O_7$ nanotubes (NTs) with a uniform diameter of 10 nm were found high-efficiency in catalyzing the hydrogenation/dehydrogenation. MgH_2–$Na_2Ti_3O_7$ NT composites could desorb 6.5 wt.% H_2 within 6 min at 573 K, absorb 6.0 wt.% H_2 within 60 s at 548 K, and could even uptake 1.5 wt.% H_2 within 30 min at a temperature as low as 323 K [140]. These enhanced absorption and desorption kinetics were attributed to the homogeneously distribution of $Na_2Ti_3O_7$ NTs in MgH_2 matrix, offering numerous diffusion channels to significantly accelerate the transportation of hydrogen atoms.

3.3. External energy field effects

The different physical fields of magnetic field and microwave field during the preparation process of Mg-based hydrogen storage alloys on its physicochemical properties including thermodynamic and kinetic characteristics have also investigated [141]. The enthalpies of Mg and Mg_2Ni in Mg–12.96 wt.%La-27.04 wt.%Ni alloy prepared by microwave-assisted activation synthesis are comparable to those of melt-spun Mg–Ni–RE alloys by nano-crystallization [142], indicating the microwave sintering has an effective effect on the thermodynamic properties of Mg–La–Ni alloys. Meng et al. [143] comparatively investigated the effect of microwave sintering and conventional sintering on properties of Nd–Mg–Ni–Fe_3O_4 alloy. It was shown that the hydrogen capacity of the samples prepared by conventional sintering was less than 4.0 wt.% at 553–623 K, whereas the samples prepared by microwave sintering exhibited higher hydrogen storage capacity (more than 4.5 wt.% at same temperature range) and wider plateau of hydriding/dehydriding. Furthermore, the enthalpy and entropy of hydrogenation for microwave sintered samples were a little lower than those of the conventionally sintered samples.

In order to investigate the magnetic field on the preparation and properties of hydrogen storage alloys, Li et al. [144, 145] designed and manufactured an experimental apparatus for magnet. The magnitude of static magnetic field on the vertical direction could change from 0 to 14 T. The nanostructured Mg_2FeH_6 was successfully prepared by controlled hydriding combustion synthesis (CHCS, with high magnetic field) [144]. The high magnetic field has an influence on the structure, morphological characterization, phase composition, crystalline size and element distribution of Mg-Fe composite. Comparison between the conventional hydriding combustion synthesis (HCS) and the CHCS was made to prepare the Mg–4 mol%$LaNi_{2.5}$ [146] and Mg–3 mol%$LaNi_3$ [145] composites. The high magnetic field changed the microstructure and phase compositions, decreased the hydriding/dehydriding temperature and the particle size of the composites. The effect of magnetic-heat treatment on the structures and electrochemical properties of $La_{0.67}Mg_{0.33}Ni_{3.0}$ [147] and $La_{0.67}Mg_{0.33}Ni_{2.5}Co_{0.5}$ [148] alloys were investigated and the results showed that the magnetic-heat treatment was helpful to the transformation of (La,Mg)Ni_3 to (La,Mg)$_2Ni_7$ and enlarged the cell volumes of alloys. The $La_{0.67}Mg_{0.33}Ni_{2.5}Co_{0.5}$ alloy obtained by magnetic-heat treatment exhibited the best discharge capacity of 324.8 $mAh{\cdot}g^{-1}$ and large capacity retention of 83.07% after 50 charge/discharge cycles. The comparative study of the CHCS and microwave synthesis to prepare Mg_2Ni was carried out [149], but the effect of magnetic field on enthalpy of (de)hydrogenation reaction was not obvious.

From above researches, it could be found that both magnetic field and microwave field introduced during the preparation process imposed a helpful effect on the microstructure, phase compositions and particle size of alloys. However, the thermodynamic properties of hydriding/dehydriding reactions did not change much. It is reasonable to expect that applying the magnetic field and microwave field not only in preparation process but also in the hydriding/dehydriding process would obviously reduce the enthalpy of reactions.

4. Kinetics mechanism

Most of hydrogen storage process are gas-solid reactions. Mg and its hydride MgH_2 have different crystal structures. Therefore, the hydrogenation and dehydrogenation of Mg-based alloys is based on the chemical reaction between Mg and MgH_2. Many researchers have analyzed the hydrogen absorption and desorption behaviors of Mg-based alloys using various kinetic models. However, seen from the reaction mechanisms, two types of models are most frequently used: diffusion-controlled reaction models [17, 150] and nucleation-growth-impingement-controlled reaction models. Jander model [28] assumes that the interface area is constant for diffusion (two- and three-dimensional diffusion are simply regarded as one-dimensional diffusion), and proposed the function of particle radius according to Fick's first law. Ginstling–Broundshtein model [29] removes the assumption of constant diffusion interface area, and give the differ-

ent functions for two dimensional cylinder and three dimensional sphere ball. The nucleation-growth-impingement models is generally regarded as classical Johnson–Mehl–Avrami–Kolomogorov (JMAK) model [30-34].

Comparing those models, a general problem has been noticed that the introduced kinetic parameters do not have clear physical meanings, such as rate constant k and rate-controlling step m. Therefore, Chou et al. [151–153] proposed a series of functions based on real physical picture to describe the hydrogenation and dehydrogenation behavior of alloys. This model mainly focuses on the physical interpreting the generalized rate constant by introducing apparent activation energy and chemical driving force [154]. At first, this model assumes that only hydrogen diffusion in hydride is slow, and the other steps all proceed very fast. Then the reacted fraction can be expressed as a function of unreacted powder radius. Introducing the relationship between hydrogen diffusion rate and the Fick's diffusion law, the preliminary model is proposed [152]

$$\xi = 1 - \left(1 - \sqrt{\frac{2D_h^{\beta}\left(C_H^{'\beta/H_2} - C_H^{''\alpha/\beta}\right)}{R_0^2 v_m}t}\right)^3 \tag{4}$$

where D_H^{β} is the diffusion coefficient, $C_H^{'\beta/H_2}$ and $C_H^{''\alpha/\beta}$ represent concentration of hydrogen in hydride β phase at the β/gas interface and at the α/β interface, R_0 is the radius of alloy particle. When the hydrogenation reaches a certain fraction φ, the required time $t_{\xi=\phi}$ is equal to [152]

$$t_{\xi=\varphi} = \frac{\left(1-(1-\varphi)^{1/3}\right)^2}{\frac{2D_H^{\beta}\left(C_H^{'\beta/H_2} - C_H^{''\alpha/\beta}\right)}{R_0^2 v_m}} \tag{5}$$

This is defined as a new concept, the "characteristic absorption time". Combining Eqs. (4) and (5), one has the simplest expression [152]

$$\xi = 1 - \left(1 - \left(1-(1-\varphi)^{1/3}\right)\sqrt{\frac{t}{t_{\xi=\varphi}}}\right)^3 \tag{6}$$

The value of Eq. (4) is that when any of the experimental point in the hydrogenation or dehydrogenation process is known, the whole kinetic curve can be predicted by substituting the known data ($t_{\xi=\varphi}$, φ). This function was used to analyze the hydrogen absorption and desorption of $Mg_{1.95}Ag_{0.05}Ni$ [152], $LaNiMg_{17}$ [56] and $La_{0.5}Ni_{1.5}Mg_{17}$ [63] alloys at different temperatures. The predicted results agreed well with experimental data which suggested that the diffusion of hydrogen through the hydrides is the rate-limiting step.

The further extension of preliminary model considered various rate-limiting steps (surface penetration of hydrogen atoms, diffusion of hydrogen atoms through the hydride, chemical reaction) and introducing the effect of temperature, hydrogen pressure and apparent activation energy. After derivation, the formulae for diffusion-controlled reaction is [151]

$$\xi = 1 - \left(1 - \sqrt{\frac{2D_H^0 K_d\left(\sqrt{P_{H_2}} - \sqrt{P_{eq}}\right)\exp\left(-\frac{E_a}{RT}\right)}{{R_0}^2 v_m}t}\right)^3 \tag{7}$$

and for other rate-controlling steps, the function format is similar

$$\xi = 1 - \left(1 - \frac{K_{rc}\left(\sqrt{P_{H_2}} - \sqrt{P_{eq}}\right)\exp\left(-\frac{E_a}{RT}\right)}{R_0 v_m}t\right)^3 \tag{8}$$

Where D_H^0 is a diffusion coefficient constant of hydrogen, P_{H_2} is the hydrogen partial pressure of hydrogen in gas, P_{eq} is hydrogen partial pressure in equilibrium with hydride, K_d and K_{rc} are equilibrium constant for diffusion and other rate-controlling steps. So far, the transformed fraction is clearly expressed as a function of time t, temperature T, hydrogen partial pressure P_{H_2}, particle radius R_0 and apparent activation energy E_a [150]. The concept of "characteristic sorption time" is further clarified as the required time of a completely hydriding or dehydriding the alloys. Therefore, the t_c is regarded as the criterion for reaction rate, which expressed as [151]

$$t_{c(d)} = \frac{{R_0}^2 v_m}{2D_H^0 K_d\left(\sqrt{P_{H_2}} - \sqrt{P_{eq}}\right)\exp\left(-\frac{E_a}{RT}\right)} \tag{9}$$

for diffusion-controlled reactions. Combining with the isothermal fitting method, this model could calculate the experimental data with higher accuracy and more explicit physical meaning. These formulae are widely used in hydrogen storage materials [81,111,155,156], ceramics oxidation [157], chemical metallurgy [158], etc. Fig. 8(a) and (b) show the hydriding kinetics of Mg_xNi_{100-x} alloys (x=33–67) and Mg_2Ni alloy respectively. The experimental data are fitted well by the diffusion kinetic model (Eq. (7)) and surface penetration model (Eq. (8)), which indicates the effect of composition and pressure on the hydriding kinetics of Mg–Ni alloys.

Then, the kinetic model is developed to describe the hydrogenation/dehydrogenation of alloys in the form of sphere, flat plate and fiber shape with considering the hydrogenation induced volume change [153]. The expression for diffusion-controlled reaction is [153]

$$\int_0^{\xi} \frac{[z-(z-1)(1-\xi)]^{1/3} - (1-\xi)^{1/3}}{3(1-\xi)^{2/3}} d\xi = \frac{D_H^0 \exp\left(-\frac{E_a}{RT}\right)K_p\left(\sqrt{P_{H_2}} - \sqrt{P_{eq}}\right)}{z{R_0}^2 v_m}t \tag{10}$$

for three-dimensional sphere ball, where z is the volume ratio of hydride to metal. The modified Chou model is applied to interpret the kinetic mechanisms of hydriding and dehydriding reactions of La–Mg–Ni alloys (Fig. 8c), and the calculated result agree well with the experimental data [159]. It indicates that the model describes the kinetic behaviors of La–Mg–Ni alloys more accurately due to the introduction of volume ratio parameter.

In addition to the geometrical contraction models, Li et al. [35,37,154] modified the classical JMAK model by taking the self-catalysis of the nucleation into consideration, and

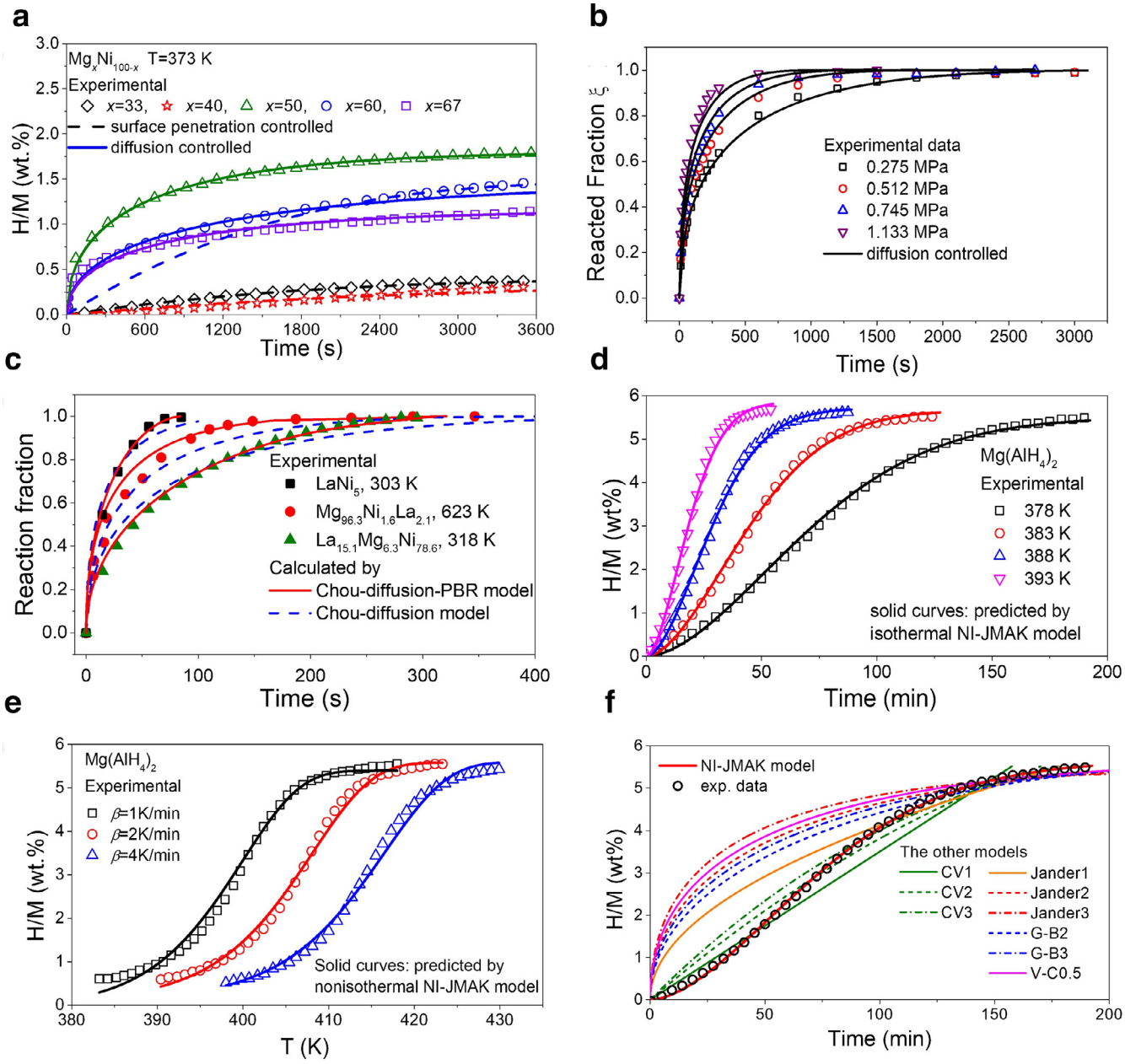

Fig. 8. The fitted curves by kinetic model comparing with experimental data: (a) the effect of Ni content on hydriding kinetics of Mg_xNi_{100-x} alloys, (b) the effect of hydrogen pressure on hydriding kinetics of Mg_2Ni alloy, (c) the effect of hydride density on the hydriding kinetics of three Mg–Ni–La alloys, (d) the effect of temperature on the dehydriding kinetics of $Mg(AlH_4)_2$, (e) the effect of heating rate on the dehydriding kinetics of $Mg(AlH_4)_2$, (f) comparison of different model-fitting curves with dehydriding kinetics of $Mg(AlH_4)_2$. Reprinted with permission [35,37,150,159].

the disadvantage of C-JMAK, linear continuous nucleation, is replaced by continuous nucleation mode. The nucleation index incorporated JMAK (NI-JMAK) model not only can analyze the isothermal hydrogen absorption and desorption behaviors through isothermal fitting methods, but also can simulate the non-isothermal behaviors by obtaining the kinetic parameters from isothermal data. The analytical form of model is [37]

$$\xi = 1 - \exp\left[- I_0^a G_0^{d/m} \mathrm{Beta}\left(a, \frac{d}{m} + 1\right) \times \exp\left(\frac{-a\Delta E_n - \frac{d}{m}E_g}{RT}\right) t^{a+\frac{d}{m}}\right] \quad (11)$$

for isothermal condition,

$$\xi = 1 - \exp\left[- I_0^a G_0^{d/m} \mathrm{Beta}\left(\frac{aE_n}{E_g}, \frac{d}{m} + 1\right) \times \exp\left(\frac{-aE_n - \frac{d}{m}E_g}{RT}\right)\left(\frac{RT^2}{\beta}\right)^{a+\frac{d}{m}}\right] \quad (12)$$

for $E_n/RT >> 0$ and non-isothermal condition, and

$$\xi = 1 - \exp\left[-I_0^a G_0^{d/m} \frac{R^{\frac{d}{m}}}{a\Delta E_g^{\frac{d}{m}} \beta^{a+\frac{d}{m}}} \times \exp\left(\frac{-\frac{d}{m}\Delta E_g}{RT}\right) T^{\frac{2d}{m}} (T - T_0)^a\right] \quad (13)$$

for $E_n/RT \approx 0$ and non-isothermal condition. Here, E_n and E_g are activation energy of nucleation and growth, a is the nucleation index, d/m is growth index, I_0 is the intrinsic nucleation rate constant, G_0 is the intrinsic growth rate and β is heating rate. Fig. 8d shows the isothermal NI-JMAK model fitted dehydriding kinetic curves of $Mg(AlH_4)_2$ alloy. With the increase of the temperature, the dehydriding rate accelerates. Fig. 8e gives the dehydriding kinetics of $Mg(AlH_4)_2$ alloy with different heating rate. It indicates that the dehydriding temperature increases with the heating rate increasing. Both the isothermal and non-isothermal cases predicted well by the NI-JMAK model. Fig. 8f illustrates the difference of isothermal NI-JMAK model with other kinetic models.

5. Summary and prospect

Hydrogen storage is a key challenge that needs to be handled with the development of storing hydrogen materials for speeding up the realization of hydrogen society. Mg-based materials are regarded as potential candidates due to the outstanding merits, such as high hydrogen storage capacity, low cost and abundant resources in the earth's crust and the sea. Unfortunately, the poor kinetics and improper thermodynamics hinder their applications for storing hydrogen, especially in the onboard storage in FCVs. In the past few decades, many approaches, such as ball milling, catalyzed chemical solution synthesis, hydrogen plasma metal reaction and in-situ formation of nanocatalyzer, have been adopted to enhance the absorption/desorption kinetics by reducing the particles size and introducing additives. Moreover, the kinetic models are provided to effectively understand the intrinsic mechanism of the materials synthesized by different methods. Among these kinetic models, the diffusion-controlled reaction model and nucleation-growth-impingement-controlled reaction model are most frequently used. In addition, an extended JMAK model, overcoming the disadvantage of classical JMAK, is developed to analyze the isothermal hydrogen absorption and desorption behaviors through isothermal fitting methods as well as the non-isothermal behaviors by obtaining the kinetics parameters from isothermal data. On the basis of this model, the parameters of activation energy of nucleation and growth, the nucleation and growth index etc. can be comprehensively determined by simultaneous analysis of isothermal and non-isothermal experimental data. It will be a great help to understand the hydrogen absorption/desorption behavior and for further development of Mg-based hydrogen storage materials.

Acknowledgments

H. Shao acknowledges the Macau Science and Technology Development Fund (FDCT) for funding (project no. 118/2016/A3 and 0062/2018/A2), and this work was also partially supported by a Start-Up Research Fund from the University of Macau (SRG2016-00088-FST). Q. Li also thanks the financial support from the National Natural Science Foundation of China (51671118), Young Elite Scientists Sponsorship Program by CAST (2017QNRC001), the "Chenguang" Program from the Shanghai Municipal Education Commission (17CG42), Science and Technology Committee of Shanghai (16520721800), the Program for Professor of Special Appointment (Eastern Scholar) by Shanghai Municipal Education Commission (No.TP2015040).

Conflict of Interest

- All authors of this manuscript have directly participated in planning, execution, and/or analysis of this study.
- The contents of this manuscript have not been copyrighted or published previously.
- The contents of this manuscript are not now under consideration for publication elsewhere.
- The contents of this manuscript will not be copyrighted, submitted, or published elsewhere while acceptance by Journal of Magnesium and Alloys.
- There are no directly related manuscripts or abstracts, published or unpublished, by any authors of this manuscript.
- The authors declare no competing financial interests or other interests that might be perceived to influence the results and/or discussion reported in this manuscript.
- I am one author signing on behalf of all co-authors of this manuscript, and attesting to the above.

References

[1] H.Y. Shao, L.Q. He, H.J. Lin, H.W. Li, Energy Technol., 6 (2018) 445–458.
[2] L. Ouyang, Y. Xu, H. Dong, L. Sun, M. Zhu, Int. J. Hydrogen Energy 34 (2009) 9671–9676.
[3] L.Z. Ouyang, Y.J. Wen, Y.J. Xu, X.S. Yang, L.X. Sun, M. Zhu, Int. J. Hydrogen Energy 35 (2010) 8161–8165.
[4] L.Z. Ouyang, J.M. Huang, H. Wang, Y.J. Wen, Q.A. Zhang, D.L. Sun, M. Zhu, Int. J. Hydrogen Energy 38 (2013) 2973–2978.
[5] L.Z. Ouyang, H. Zhong, Z.M. Li, Z.J. Cao, H. Wang, J.W. Liu, X.K. Zhu, M. Zhu, J. Power Sources 269 (2014) 768–772.
[6] J. Huang, R. Duan, L. Ouyang, Y. Wen, H. Wang, M. Zhu, Int. J. Hydrogen Energy 39 (2014) 13564–13568.
[7] M. Huang, L. Ouyang, H. Wang, J. Liu, M. Zhu, Int. J. Hydrogen Energy 40 (2015) 6145–6150.
[8] H. Zhong, H. Wang, J. Liu, D. Sun, F. Fang, Q. Zhang, L. Ouyang, M. Zhu, J. Alloys Compd. 680 (2016) 419–426.
[9] A. Zaldívar-Cadena, I. Díaz-Peña, J. Cabañas-Moreno, J. Magnes. Alloys 1 (2013) 292–296.
[10] L. Ouyang, W. Chen, J. Liu, M. Felderhoff, H. Wang, M. Zhu, Adv. Energy Mater. 7 (2017) 1700299.
[11] W. Chen, L. Ouyang, J. Liu, X. Yao, H. Wang, Z. Liu, M. Zhu, J. Power Sources 359 (2017) 400–407.
[12] H. Zhong, L.Z. Ouyang, J.S. Ye, J.W. Liu, H. Wang, X.D. Yao, M. Zhu, Energy Storage Mater. 7 (2017) 222–228.

[13] L. Schlapbach, A. Züttel, Nature, World Scientific, 2011, pp. 353–358.
[14] G. Xia, Y. Tan, X. Chen, D. Sun, Z. Guo, H. Liu, L. Ouyang, M. Zhu, X. Yu, Adv. Mater. 27 (2015) 5981–5988.
[15] S.I. Orimo, Y. Nakamori, J.R. Eliseo, A. Züttel, C.M. Jensen, Chem. Rev. 107 (2007) 4111–4132.
[16] J. Li, B. Li, H. Shao, W. Li, H. Lin, Catalyst 8 (2018) 89.
[17] H. Shao, G. Xin, J. Zheng, X. Li, E. Akiba, Nano Energy 1 (2012) 590–601.
[18] E.S. Cho, A.M. Ruminski, S. Aloni, Y.-S. Liu, J. Guo, J.J. Urban, Nat. Commun. 7 (2016) 10804.
[19] H. Zhang, X. Zheng, X. Tian, Y. Liu, X. Li, Prog. Nat. Sci. Mater. 27 (2017) 50–57.
[20] N. Mushnikov, A. Ermakov, M. Uimin, V. Gaviko, P. Terent'ev, A. Skripov, A. Tankeev, A. Soloninin, A. Buzlukov, Phys. Met. Metallogr. 102 (2006) 421–431.
[21] H.E. Kissinger, Anal. Chem. 29 (1957) 1702–1706.
[22] H. Wang, H. Lin, W. Cai, L. Ouyang, M. Zhu, J. Alloys Compd. 658 (2016) 280–300.
[23] H. Shao, M. Felderhoff, F. Schuth, Int. J. Hydrogen Energy 36 (2011) 10828–10833.
[24] R.W.P. Wagemans, J.H. van Lenthe, P.E. de Jongh, A.J. van Dillen, K.P. de Jong, J. Am. Chem. Soc. 127 (2005) 16675–16680.
[25] Q. Li, K. Chou, Q. Lin, L. Jiang, F. Zhan, Int. J. Hydrogen Energy 29 (2004) 843–849.
[26] J. Liu, X. Zhang, Q. Li, K. Chou, K. Xu, Int. J. Hydrogen Energy 34 (2009) 1951–1957.
[27] Q. Li, L. Jiang, K. Chou, Q. Lin, F. Zhan, X. Lu, J. Zhang, J. Alloys Compd. 399 (2005) 101–105.
[28] W. Jander, Z. Anorg, Allg. Chem. 163 (1927) 1–30.
[29] A. Ginstling, B. Brounshtein, Zhur. Priklad. Khim. 23 (1950).
[30] J. William, R. Mehl, Trans. Am. Inst. Min. Engrs 135 (1939) 416–442.
[31] M. Avrami, J. Chem. Phys. 9 (1941) 177–184.
[32] M. Avrami, J. Chem. Phys. 8 (1940) 212–224.
[33] M. Avrami, J. Chem. Phys., 7 (1939) 1103–1112.
[34] A.N. Kolmogorov, Bull. Acad. Sci. USSR, Math. Ser. 1 (1937) 355–359.
[35] Y. Pang, Q. Li, Scr. Mater. 130 (2017) 223–228.
[36] X. An, Y. Pan, Q. Luo, X. Zhang, J. Zhang, Q. Li, J. Alloys Compd. 506 (2010) 63–69.
[37] Y. Pang, D. Sun, Q. Gu, K. Chou, X. Wang, Q. Li, Cryst. Growth Des. 16 (2016) 2404–2415.
[38] G. Wu, J. Zhang, Q. Li, Y. Wu, K. Chou, X. Bao, Comput. Mater. Sci. 49 (2010) S144–S149.
[39] G. Wu, J. Zhang, Q. Li, K. Chou, Int. J. Hydrogen Energy 36 (2011) 12923–12931.
[40] H. Shao, J. Matsuda, H. Li, E. Akiba, A. Jain, T. Ichikawa, Y. Kojima, Int. J. Hydrogen Energy 38 (2013) 7070–7076.
[41] H. Shao, K. Asano, H. Enoki, E. Akiba, Scr. Mater. 60 (2009) 818–821.
[42] L. Ouyang, Z. Cao, H. Wang, J. Liu, D. Sun, Q. Zhang, M. Zhu, J. Alloys Compd. 586 (2014) 113–117.
[43] L. Ouyang, S. Ye, H. Dong, M. Zhu, Appl. Phys. Lett. 90 (2007) 021917.
[44] L. Ouyang, Z. Cao, L. Li, H. Wang, J. Liu, D. Min, Y. Chen, F. Xiao, R. Tang, M. Zhu, Int. J. Hydrogen Energy 39 (2014) 12765–12772.
[45] L. Ouyang, Z. Cao, H. Wang, J. Liu, D. Sun, Q. Zhang, M. Zhu, Int. J. Hydrogen Energy 38 (2013) 8881–8887.
[46] Z. Cao, L. Ouyang, Y. Wu, H. Wang, J. Liu, F. Fang, D. Sun, Q. Zhang, M. Zhu, J. Alloys Compd. 623 (2015) 354–358.
[47] X. Ding, Y. Li, F. Fang, D. Sun, Q. Zhang, J. Mater. Chem. A 5 (2017) 5067–5076.
[48] B. Bogdanović, S.t. Liao, M. Schwickardi, P. Sikorsky, B. Spliethoff, Angew. Chem. Int. Ed. 19 (1980) 818–819.
[49] H. Shao, M. Felderhoff, F. Schüth, C. Weidenthaler, Nanotechnology 22 (2011) 235401.
[50] H. Shao, T. Liu, Y. Wang, H. Xu, X. Li, J. Alloys Compd. 465 (2008) 527–533.
[51] H. Shao, T. Liu, X. Li, Nanotechnology 14 (2003) L1.
[52] H. Shao, H. Xu, Y. Wang, X. Li, J. Solid State Chem. 177 (2004) 3626–3632.
[53] H. Shao, Y. Wang, H. Xu, X. Li, J. Solid State Chem. 178 (2005) 2211–2217.
[54] S. Ohno, J. Japan. Inst. Metals 48 (1984) 640–646.
[55] Q. Li, K. Chou, Q. Lin, L. Jiang, F. Zhan, J. Mater. Sci. 39 (2004) 6987–6991.
[56] Q. Li, K. Chou, K. Xu, Q. Lin, L. Jiang, F. Zhan, J. Alloys Compd. 387 (2005) 86–89.
[57] Q. Li, Q. Lin, K. Chou, L. Jiang, F. Zhan, J. Mater. Res. 19 (2004) 2871–2876.
[58] Q. Li, K. Chou, K. Xu, Q. Lin, L. Jiang, F. Zhan, Intermetallics 14 (2006) 1386–1390.
[59] Q. Li, Q. Lin, K. Chou, L. Jiang, F. Zhan, Intermetallics 12 (2004) 1293–1298.
[60] Q. Li, K. Chou, Q. Lin, L. Jiang, F. Zhan, J. Alloys Compd. 373 (2004) 122–126.
[61] Q. Li, Q. Lin, L. Jiang, K. Chou, J. Alloys Compd. 368 (2004) 101–105.
[62] Q. Li, Q. Lin, L. Jiang, K. Chou, F. Zhan, Q. Zheng, J. Mater. Sci. 20 (2004) 209–212.
[63] Q. Li, K. Chou, L. Jiang, Q. Lin, G. Lin, X. Lu, J. Zhang, Int. J. Hydrogen Energy 31 (2006) 497–503.
[64] L. Yao, H. Han, Y. Liu, Y. Zhu, Y. Zhang, L. Li, Prog. Nat. Sci. Mater. 28 (2018) 7–14.
[65] Y. Zhu, S. Luo, H. Lin, Y. Liu, Y. Zhu, Y. Zhang, L. Li, J. Alloys Compd. 712 (2017) 44–49.
[66] S. Luo, H. Han, H. Huang, J. Zhang, Y. Liu, Y. Zhu, Y. Zhang, B. Xu, L. Li, J. Alloys Compd. 750 (2018) 490–498.
[67] Y. Jia, C. Sun, S. Shen, J. Zou, S.S. Mao, X. Yao, Renew. Sustain. Energy Rev. 44 (2015) 289–303.
[68] Z. Ma, J. Zhang, Y. Zhu, H. Lin, Y. Liu, Y. Zhang, D. Zhu, L. Li, ACS Appl. Energy Mater. 1 (2018) 1158–1165.
[69] J. Zhang, Y. Zhu, X. Zang, Q. Huan, W. Su, D. Zhu, L. Li, J. Mater. Chem. A 4 (2016) 2560–2570.
[70] Y. Tan, Y. Zhu, L. Li, Chem. Commun. 51 (2015) 2368–2371.
[71] J. Yuan, Y. Zhu, L. Li, Chem. Commun. 50 (2014) 6641–6644.
[72] W. Li, C. Li, H. Ma, J. Chen, J. Am. Chem. Soc. 129 (2007) 6710–6711.
[73] B. Peng, L. Li, W. Ji, F. Cheng, J. Chen, J. Alloys Compd. 484 (2009) 308–313.
[74] J. Zhang, Y. Zhu, H. Lin, Y. Liu, Y. Zhang, S. Li, Z. Ma, L. Li, Adv. Mater. 29 (2017) 1700760.
[75] W. Klement, R.H. Willens, P. Duwez, Nature 187 (1960) 869–870.
[76] H.J. Lin, M. He, S.P. Pan, L. Gu, H.W. Li, H. Wang, L.Z. Ouyang, J.W. Liu, T.P. Ge, D.P. Wang, W.H. Wang, E. Akiba, M. Zhu, Acta Mater. 120 (2016) 68–74.
[77] W. Jiao, P. Liu, H. Lin, W. Zhou, Z. Wang, T. Fujita, A. Hirata, H.W. Li, M. Chen, Chem. Mater. 29 (2017) 4478–4483.
[78] L. Ouyang, X. Yang, M. Zhu, J. Liu, H. Dong, D. Sun, J. Zou, X. Yao, J. Phys. Chem. C 118 (2014) 7808–7820.
[79] J. Liu, C. Zou, H. Wang, L. Ouyang, M. Zhu, Int. J. Hydrogen Energy 38 (2013) 10438–10445.
[80] Q. Zhang, D. Liu, Q. Wang, F. Fang, D. Sun, L. Ouyang, M. Zhu, Scr. Mater. 65 (2011) 233–236.
[81] Q. Luo, Q. Gu, J. Zhang, S. Chen, K. Chou, Q. Li, Sci. Rep. 5 (2015) 15385.
[82] Q. Li, Q. Luo, Q. Gu, J. Mater. Chem. A 5 (2017) 3848–3864.
[83] Y. Li, Q. Gu, Q. Li, T. Zhang, Scr. Mater. 127 (2017) 102–107.
[84] Q. Li, Y. Li, B. Liu, X. Lu, T. Zhang, Q. Gu, J. Mater. Chem. A 5 (2017) 17532–17543.
[85] Q. Luo, Q. Gu, B. Liu, T. Zhang, W. Liu, Q. Li, J. Mater. Chem. A 6 (2018) 23308–23317.
[86] H. Shao, Energies 10 (2017) 1767.
[87] H. Shao, Y. Wang, H. Xu, X. Li, Mater. Sci. Eng. B 110 (2004) 221–226.
[88] Z. Wei, L. Rosa, K. Wang, M. Endo, S. Juodkazis, B. Ohtani, E. Kowalska, Appl. Catal. B Environ. 206 (2017) 393–405.

[89] C. Shen, K.F. Aguey-Zinsou, Energies 9 (2016) 1073.
[90] V. Berube, G. Radtke, M. Dresselhaus, G. Chen, Int. J. Energ. Res. 31 (2007) 637–663.
[91] W. Oelerich, T. Klassen, R. Bormann, J. Alloys Compd. 315 (2001) 237–242.
[92] H. Lin, J. Tang, Q. Yu, H. Wang, L. Ouyang, Y. Zhao, J. Liu, W. Wang, M. Zhu, Nano Energy 9 (2014) 80–87.
[93] S. Milošević, S. Kurko, L. Pasquini, L. Matović, R. Vujasin, N. Novaković, J.G. Novaković, J. Power Sources 307 (2016) 481–488.
[94] N. Hanada, T. Ichikawa, H. Fujii, J. Phys. Chem. B 109 (2005) 7188–7194.
[95] E.S. Cho, A.M. Ruminski, Y.S. Liu, P.T. Shea, S. Kang, E.W. Zaia, J.Y. Park, Y.D. Chuang, J.M. Yuk, X. Zhou, Adv. Funct. Mater. 27 (2017) 1704316.
[96] H. Shao, T. Liu, X. Li, L. Zhang, Scr. Mater. 49 (2003) 595–599.
[97] H. Shao, K. Asano, H. Enoki, E. Akiba, J. Alloys Compd. 477 (2009) 301–306.
[98] P. Meena, R. Singh, V. Sharma, I. Jain, J. Magnes, Alloys (2018).
[99] Z. Wang, H. Zhou, R. Zou, Z. Gu, J. Mater. Sci. Technol. 21 (2005) 119–122.
[100] Z. Yuan, G. Lu, B. Liao, Y. Lei, J. Mater. Sci. Technol. 21 (2005) 231–233.
[101] J. Mao, J. Zou, C. Lu, X. Zeng, W. Ding, J. Power Sources 366 (2017) 131–142.
[102] H. Lin, J. Matsuda, H. Li, M. Zhu, E. Akiba, J. Alloys Compd. 645 (2015) S392–S396.
[103] M. Ismail, Energy 79 (2015) 177–182.
[104] I. Malka, T. Czujko, J. Bystrzycki, Int. J. Hydrogen Energy 35 (2010) 1706–1712.
[105] G. Barkhordarian, T. Klassen, R. Bormann, Scr. Mater. 49 (2003) 213–217.
[106] N. Mustafa, M. Ismail, J. Alloys Compd. 695 (2017) 2532–2538.
[107] A. Revesz, M. Gajdics, T. Spassov, Int. J. Hydrogen Energy 38 (2013) 8342–8349.
[108] S.D. House, J.J. Vajo, C. Ren, A.A. Rockett, I.M. Robertson, Acta Mater. 86 (2015) 55–68.
[109] S.A. Jin, J.H. Shim, J.P. Ahn, Y.W. Cho, K.W. Yi, Acta Mater. 55 (2007) 5073–5079.
[110] L. Xie, Y. Liu, Y.T. Wang, J. Zheng, X.G. Li, Acta Mater. 55 (2007) 4585–4591.
[111] X. Han, Y. Qian, W. Liu, D. Chen, K. Yang, J. Mater. Sci. 32 (2016) 1332–1338.
[112] R.V. Denys, A.A. Poletaev, J.K. Solberg, B.P. Tarasov, V.A. Yartys, Acta Mater. 58 (2010) 2510–2519.
[113] H.J. Lin, L.Z. Ouyang, H. Wang, D.Q. Zhao, W.H. Wang, D.L. Sun, M. Zhu, Int. J. Hydrogen Energy 37 (2012) 14329–14335.
[114] L. Pei, S. Han, J. Wang, L. Hu, X. Zhao, B. Liu, Mater. Sci. Eng. B 177 (2012) 1589–1595.
[115] L.J. Huang, G.Y. Liang, Z.B. Sun, J. Alloys Compd. 421 (2006) 279–282.
[116] Z. Yuan, B. Zhang, Y. Zhang, S. Guo, X. Dong, D. Zhao, J. Mater. Sci. Technol. 34 (2018) 1851–1858.
[117] H.B. Lu, C.K. Poh, L.C. Zhang, Z.P. Guo, X.B. Yu, H.K. Liu, J. Alloys Compd. 481 (2009) 152–155.
[118] J. Zou, H. Sun, X. Zeng, G. Ji, W. Ding, J. Nanomater. 2012 (2012) 2.
[119] X. Chen, J. Zou, X. Zeng, W. Ding, J. Alloys Compd. 701 (2017) 208–214.
[120] L. Zhang, X. Xiao, C. Xu, J. Zheng, X. Fan, J. Shao, S. Li, H. Ge, Q. Wang, L. Chen, J. Phys. Chem. C 119 (2015) 8554–8562.
[121] H. Zhou, Y. Wang, Q. Yao, J. Alloys Compd. 407 (2006) 129–131.
[122] H. Zhou, S. Zhang, Q. Yao, W. Li, J. Alloys Compd. 429 (2007) 116–118.
[123] Q. Yao, H. Zhou, Z. Wang, J. Alloys Compd. 421 (2006) 117–119.
[124] S. De Negri, M. Giovannini, A. Saccone, J. Alloys Compd. 439 (2007) 109–113.
[125] S. De Negri, M. Giovannini, A. Saccone, J. Alloys Compd. 397 (2005) 126–134.
[126] S. De Negri, M. Giovannini, A. Saccone, J. Alloys Compd. 427 (2007) 134–141.
[127] Q. Li, X. Zhang, X. An, S. Chen, J. Zhang, J. Alloys Compd. 509 (2011) 2478–2486.
[128] K. Wu, Q. Luo, S. Chen, Q. Gu, K. Chou, X. Wang, Q. Li, Int. J. Hydrogen Energy 41 (2016) 1725–1735.
[129] Z. Wang, Q. Luo, S. Chen, K. Chou, Q. Li, J. Alloys Compd. 649 (2015) 1306–1314.
[130] J. Mao, Z. Guo, X.B. Yu, H. Liu, Z. Wu, J. Ni, Int. J. Hydrogen Energy 35 (2010) 4569–4575.
[131] L. Wei, H. Sun, F. Song, Z. Cui, Y. Zhu, L. Li, J. Alloys Compd. 698 (2017) 913–920.
[132] Y. Zhang, X. Xiao, B. Luo, X. Huang, M. Liu, L. Chen, J. Phys. Chem. C 122 (2018) 2528–2538.
[133] J. Zou, X. Zeng, Y. Ying, P. Stephane, W. Ding, Int. J. Hydrogen Energy 37 (2012) 13067–13073.
[134] J. Zou, X. Zeng, Y. Ying, X. Chen, H. Guo, S. Zhou, W. Ding, Int. J. Hydrogen Energy 38 (2013) 2337–2346.
[135] C. Lu, J. Zou, X. Zeng, W. Ding, Int. J. Hydrogen Energy 42 (2017) 15246–15255.
[136] J. Zou, S. Long, L. Zhang, C. Lu, X. Chen, X. Zeng, W. Ding, Mater. Trans. 55 (2014) 1156–1160.
[137] C. Lu, J. Zou, X. Shi, X. Zeng, W. Ding, Int. J. Hydrogen Energy 42 (2017) 2239–2247.
[138] X. Xiao, C. Xu, J. Shao, L. Zhang, T. Qin, S. Li, H. Ge, Q. Wang, L. Chen, J. Mater. Chem. A 3 (2015) 5517–5524.
[139] X. Huang, X. Xiao, W. Zhang, X. Fan, L. Zhang, C. Cheng, S. Li, H. Ge, Q. Wang, L. Chen, Phys. Chem. Chem. Phys. 19 (2017) 4019–4029.
[140] L. Zhang, L. Chen, X. Fan, X. Xiao, J. Zheng, X. Huang, J. Mater. Chem. A 5 (2017) 6178–6185.
[141] J. Meng, X. Wang, K. Chou, Q. Li, Metall. Mater. Trans. A 44 (2013) 58–67.
[142] K. Tanaka, Y. Kanda, M. Furuhashi, K. Saito, K. Kuroda, H. Saka, J. Alloys Compd. 293 (1999) 521–525.
[143] J. Meng, Y. Pan, Q. Luo, X. An, Y. Liu, Q. Li, K. Chou, Int. J. Hydrogen Energy 35 (2010) 8310–8316.
[144] Q. Li, J. Liu, K. Chou, G. Lin, K. Xu, J. Alloys Compd. 466 (2008) 146–152.
[145] Q. Li, K. Xu, K. Chou, X. Lu, J. Zhang, G. Lin, Intermetallics 15 (2007) 61–68.
[146] Q. Li, X. Lu, K. Chou, K. Xu, J. Zhang, S. Chen, Int. J. Hydrogen Energy 32 (2007) 1875–1884.
[147] Z. Yang, Q. Li, X. Zhao, J. Alloys Compd. 558 (2013) 99–104.
[148] X. Zhao, Q. Li, K. Chou, H. Liu, G. Lin, J. Alloys Compd. 473 (2009) 428–432.
[149] Q. Li, J. Liu, Y. Liu, K. Chou, Int. J. Hydrogen Energy 35 (2010) 3129–3135.
[150] Q. Luo, X. An, Y. Pan, X. Zhang, J. Zhang, Q. Li, Int. J. Hydrogen Energy 35 (2010) 7842–7849.
[151] K. Chou, K. Xu, Intermetallics 15 (2007) 767–777.
[152] K. Chou, Q. Li, Q. Lin, L. Jiang, K. Xu, Int. J. Hydrogen Energy 30 (2005) 301–309.
[153] K. Chou, Q. Luo, Q. Li, J. Zhang, Intermetallics 47 (2014) 17–22.
[154] Y. Pang, Q. Li, Int. J. Hydrogen Energy 41 (2016) 18072–18087.
[155] X. Cui, Q. Li, K. Chou, S. Chen, G. Lin, K. Xu, Intermetallics 16 (2008) 662–667.
[156] H. Zhou, X. Lan, Z. Wang, Q. Yao, C. Ni, W. Liu, Int. J. Hydrogen Energy 37 (2012) 13178–13184.
[157] K. Chou, X. Hou, J. Am. Ceram. Soc. 92 (2009) 585–594.
[158] Z.Y. Chen, L.Z. Bian, Z.Y. Yu, L.J. Wang, F.S. Li, K.C. Chou, Int. J. Min. Met. Mater. 25 (2018) 226–235.
[159] Y. Pang, Q. Li, Q. Li, Q. Luo, K. Chou, Int. J. Hydrogen Energy 41 (2016) 9183–9190.